HHS Public Access

Author manuscript

Nat Neurosci. Author manuscript; available in PMC 2009 September 01.

Published in final edited form as:

Nat Neurosci. 2009 March ; 12(3): 286–294. doi:10.1038/nn.2265.

Slow glycinergic transmission mediated by transmitter pooling

Veeramuthu Balakrishnan, **Sidney P. Kuo**, **Patrick D. Roberts**, and **Laurence O. Trussell**[*]

Oregon Hearing Research Center and Vollum Institute, 3181 S.W. Sam Jackson Park Road, Portland, Oregon 97239

Abstract

Most fast-acting neurotransmitters are rapidly cleared from synaptic regions. This feature isolates synaptic sites, rendering the timecourse of synaptic responses independent of the number of active synapses. We describe a striking exception at glycinergic synapses on granule cells of the rat dorsal cochlear nucleus. The duration of IPSCs was dependent on the number of presynaptic axons that were stimulated and on the number of vesicles released from each axon. Increasing stimulus number or frequency, or blocking glycine uptake, slowed synaptic decays, while a low-affinity competitive antagonist of GlyRs accelerated IPSC decay. These effects could be explained by unique features of GlyRs when activated by pooling of glycine across synapses. Functionally, increasing the number of IPSPs markedly lengthened the period of spike inhibition following cessation of presynaptic stimulation. Thus, temporal properties of inhibition can be controlled by activity levels in multiple presynaptic cells or by adjusting release probability at individual synapses.

Keywords

granule cell; cochlear nucleus; GlyR; transmitter pooling; multivesicular release

Introduction

The duration of postsynaptic currents depends on the kinetics of the neurotransmitter-receptor interaction 1 and the process of exocytosis 2. Channel gating, affinity, and desensitization may determine how single synaptic events participate in neural computations by controlling the duration of receptor activation 3-7. Under some conditions however, the clearance of transmitter appears to be delayed, leading to rebinding of transmitter and a slowing of the synaptic decay, particularly at multi-release site synapses 8-12. Developmental changes in synaptic structure or glial apposition can modify the profile of clearance 13. At mature inhibitory and excitatory synapses, pooling of transmitter sufficient to reactivate postsynaptic receptors appears most prominent when transmitter uptake systems are blocked (e.g. ref 14). Thus, it is generally presumed that under normal conditions, slower synaptic decay rates at inhibitory synapses must reflect either receptor

[*]**Address correspondence to:** Laurence O. Trussell Oregon Hearing Research Center and Vollum Institute 3181 S.W. Sam Jackson Park Road, Portland, Oregon 97239 Email: trussell@ohsu.edu.

subunit composition 15 or the activity of synapses prone to asynchronous release 16. In either case, these mechanisms do not have much power to grade synaptic decays on a fast time scale or over a wide range.

Glycinergic synapses mediate rapid transmission in the brainstem and spinal cord, with typical IPSC decay times of only a few ms 17. Glycine receptors (GlyRs) feature multiple binding sites, and their occupancy has distinctive effects upon gating kinetics 18-20. Well-timed glycinergic inhibition plays a crucial role in determining the synaptic output in several brain regions, particularly in the auditory system, where the precise timing of inhibition is critical to information processing 21. It is generally believed that the decay of glycinergic synaptic currents solely reflects the burst or open duration of GlyR channels 5, 6, 20, 22. The relatively incomplete desensitization exhibited by GlyRs 5, 23 and the slow turnover rates of neurotransmitter transporters 24, 25 suggests the possibility that clearance might determine IPSC decay in some cases. We studied the determinants of glycinergic IPSCs decay in granule cells of the dorsal cochlear nucleus (DCN). The DCN is a laminated structure resembling the cerebellar cortex, in which glycinergic and glutamatergic synaptic activity controls the convergence and plasticity of different sensory streams 26 (Fig 1a,b). DCN granule cells receive strong glycinergic input presumably from Golgi and/or stellate cells 27. In contrast to the rapid decays of most glycinergic IPSCs, typically just a few ms in the adult auditory brainstem 28, 29, glycinergic events last more than 10-times longer in granule cells 27. Varying the frequency and intensity of exocytosis, and interfering with glycine-receptor interactions with a low-affinity competitive antagonist, revealed that transmitter pooling controls the duration of inhibition in an activity-dependent manner.

Results

Correlation between amplitude and decay time of glycinergic IPSCs

For a given stimulus strength, glycinergic IPSCs varied widely in amplitude, suggesting stochastic fluctuation in the number of vesicles released from trial-to-trial (Fig 1d). IPSCs, fitted with a double-exponential function, had an average τ_{fast} of 13±2 msec, τ_{slow} of 59±8 msec and %fast of 60±4 (n=46). For each cell, the IPSC decay time was generally longest for the largest events (Fig 1d,e). Indeed, IPSC amplitude and decay time were positively correlated within cells (Fig. 1e, mean r=0.60±0.10; n=6; $P<0.02$ for 5/6 cells). By contrast, the 10-90% rise times of the IPSCs displayed no correlation (mean r=0.16±0.08; n=6; $P>0.2$ for 6/6 cells; Fig. 1f). The lack of correlation with rise time suggests that larger events are not associated with poorly synchronized release, and that extrasynaptic receptors do not contribute to peak current. Rather, these data suggest that fluctuation in the amount of transmitter release might lead to variation in the exposure time of receptors to glycine.

The decay time also correlated with the number of axonal inputs activated during the IPSC. Evoked IPSC amplitude increased with stimulus intensity, typically in 2-4 steps, suggesting that each granule cell is contacted by several glycinergic axonal inputs (Fig 1g). Consistently, this increase in amplitude was linearly correlated with decay time (Fig 1h,i). Because granule cells are electrically compact, this slowing of the decay could not be due to escape from voltage clamp 27, 30. Rather, these observations are consistent with the idea that increasing the number of active synapses leads to transmitter pooling.

Pooling of transmitter release following repetitive exocytosis

In order to determine if such pooling of transmitter could be enhanced by repetitive synaptic stimuli, synapses were activated by varying the number (1 to 10; at 100 Hz) or frequency (20-200 Hz) of stimuli. As shown in Figure 1j,k, the decay time positively correlated with the number of stimuli (r=0.9; P<0.0001; slope=4.8 ms/added stimulus). Increasing stimuli from one to ten increased the decay by 176±27% (n=5; P=0.0029). Elevating the stimulus frequency by ten times, from 20 to 200 Hz, also increased the decay time, by 158±44% (Fig. 1l,m; n=7; P=0.012). In order to test whether the increased decay time following trains could be due to modulatory effects of GABA or glutamate released from other nerve fibers, which might cause a Ca^{2+} rise in the postsynaptic cell, we repeated single and 100 Hz train stimuli in the presence of 20 μM each of (*RS*)-α-ethyl-4-carboxyphenylglycine (E4CPG) and (*RS*)-α -cyclopropyl-4-phosphonophenylglycine (CPPG) to block group I-III mGluRs and 10 μM CGP-55845 to block $GABA_B$ receptors. In 7 experiments, train stimulation increased the decay time by 115±22%, indicating that slower decays are not produced by activation of such modulatory pathways (data not shown). Finally, we tested whether the slow glycine IPSC could reflect an artifact of the high intracellular Cl^- used in the voltage clamp experiments 31 and found that slow decays remained when Cl^- was reduced to 10 mM (Single IPSC decay 17.4±4.1 ms; IPSC decay after train 56.6±11.9 ms, n=5).

The increased decay time following train-evoked IPSCs might result from enhancement of delayed quantal releases, as has been shown at some GABAergic synapses 16. However, such delayed releases were not as prominent as in GABAergic synapses, and so were not likely to be of sufficient frequency to slow the current decay. To determine if asynchronous release could have been detected, 8 mM Sr^{2+} was substituted for extracellular Ca^{2+} and synaptic stimuli were delivered at low or high frequency. In Sr^{2+}, asynchronous quantal releases were clearly observed after single or multiple stimuli (Fig 2a,b), and exhibited a marked increase in frequency over the sparse delayed events seen in control solution. Delayed quantal release events were sampled, aligned and averaged to assess their amplitude and duration. The decay of quantal events was compared to that of single and train-evoked responses in normal Ca^{2+} solutions in the same cells, revealing that quantal currents decayed nearly twice as fast as the response to single presynaptic stimuli (Fig 2c,d). Given the mean size of these events (33.5±16.5 pA, n=5 cells, Fig 2c), they would have been visible during the decay of evoked currents in Ca^{2+}-containing solutions if they were responsible for slowing the decay by several fold. However, in six cells in the absence of Sr^{2+}, we detected by eye an average of only 0.17±0.06 quantal events per trace during a 500 ms window after the train (not shown; 506 traces total). This was determined after “linearizing” the current decay after a train by subtracting a fitted biexponential curve from each trace. While some slowing of the evoked response is expected due to the profile of exocytosis, such asynchrony is probably not great, as the rise time of quantal and evoked events were not significantly different (Fig 2d).

We tested this further by using the average amplitude and decay of quantal responses recorded in Sr^{2+} to deconvolve the release timecourse expected if the slow IPSC decay was due solely to release rate and channel kinetics (Fig 2e,f). We examined the release rate after the 10^{th} stimulus in a train, when the current had decayed by 63%, a point where quantal

releases should have been easily apparent from the baseline. This analysis predicted an average release rate at that time of 0.18±0.02 per ms, or roughly one event every 5.6 ms (mean from three neurons, with three measurements/cell), much higher than the measured rate of 0.17 releases/500 ms. It may be argued that many releases were undetected because of a high signal-to-noise ratio. However the noise level was quite low, and in some cells it was possible to easily resolve single GlyR channel currents underlying the IPSCs (Fig 2g,h), as shown previously 27. Thus, in a single stimulus or with repeated stimuli, the slower IPSC decay is due to a more gradual transmitter clearance rather than a gradually decaying rate of release.

Release probability influences the decay time

If enhanced synaptic activity leads to slowing of transmitter removal and consequently of the synaptic decay time, then release probability and decay time should also correlate. To test this idea, we compared the IPSCs evoked in different extracellular Ca^{2+} concentrations. Raising the release probability by increasing Ca^{2+} between 1 mM and 4 mM increased the mean synaptic decay time (Fig. 3a,b). Halving bath Ca^{2+} from 2 to 1 mM reduced the decay time by 26±3% and the amplitude by 52±5% ($P<0.001$ for both, n=6). Doubling Ca^{2+} nearly doubled both decay time and amplitude (80±16% and 87±19% increase, respectively, $P<0.01$, n=5). Interestingly, the extent of changes in amplitude and decay time induced by changes in Ca^{2+} resembled those seen with changes in stimulus strength (Fig 1h,i). This relationship implies that release sites from different axons are so close that increasing the number of activated axons or the probability of release from each axon has an equivalent effect on the decay time. The relation between amplitude and decay time also predicted well the mean values obtained for quantal currents recorded in Sr^{2+} solutions described earlier (Fig 2b).

Glycine transporters shape the IPSC

Transmitter spillover between synapses is often enhanced after blockade of transmitter transporters 3, 14, 32, 33. Given the dominant role of slow glycine clearance shaping IPSCs in granule cells, we asked if uptake systems play any role in regulating the decay of glycinergic events. Upon bath application of ALX-5407 (20 μM), a blocker of the glial glycine transporter (GlyT1) 34, the decay time of glycinergic IPSCs upon single stimulation increased by 43±10% (19.1±3.1 ms to 26.5±4.4 ms, n=8; P=0.019, paired t-test), as shown in Fig S1. By contrast, no significant change in the amplitude was apparent (29±19% change; n=8; P=0.145). ALX-5407 also increased the decay following trains of 10 stimuli at 100 Hz by 36±9% (44±5 to 60±8 ms; n=7; P=0.009, paired t-test). A second series of experiments were performed with 20 μM ORG-25543, an antagonist of the neuronal glycine transporter, GlyT2 35. As with the GlyT1 antagonist, the decay time after single or 100-Hz train stimuli was lengthened following blockade of neuronal glycine uptake (singles: from 17.5±2.1 ms to 23.7±2.6 ms, 43±20% increase, n=8, P=0.03, paired t-test; trains: from 52.9±7.5 ms to 73.6±12.1 ms, 40±12%, n=5, P=0.04, paired t-test) with no change in amplitude (P=0.66) (Fig S1). Thus, glial and neuronal glycine transporters play a role in shaping synaptic responses, but do not prevent transmitter rebinding and reactivating receptors after single synaptic stimuli.

Multivesicular release determines peak IPSC amplitude

The effect of increasing stimulus strength on IPSC decay is likely due to the pooling of transmitter from neighboring release sites. However, the slowing of IPSC decays after increase in release probability could be explained either by pooling or by multivesicular release, in which multiple vesicles are released from individual release sites; either situation could in principle lengthen the time for transmitter to fall below the level needed to activate receptors. SR-95531 (gabazine), a well-known $GABA_A$ receptor antagonist, has been shown to act as a low-affinity competitive antagonist of native or heterologously expressed GlyRs 20, 36, 37. We used SR-95531 to test for multivesicular release and to probe transmitter lifetime in the cleft. The mean amplitude of IPSCs in 2 mM bath Ca^{2+} decreased by 71±2% (n=10; *P*=0.0005) in the presence of 300 μM SR-95531, as illustrated in Fig. 4a,b. The effectiveness of the antagonist was then tested in 1 mM or 4 mM Ca^{2+}, revealing that block by SR-95531 increased when quantal release was reduced (Fig 4b). These data indicate that multiple vesicles must be released at individual release sites in response to single stimuli in 2 mM bath Ca^{2+}. Having established the presence of mutivesicular release we next then examined the degree of inhibition by SR-95531 in 2 mM bath Ca^{2+} in the presence of ALX-5407 (20 μM) and ORG-25543 (20 μM). This approach explored the view that the apparent competition between the transmitter and antagonist on the peak current is influenced by spillover of transmitter between synaptic sites. However, in the presence of both blockers the percent inhibition was 68±6% (n=4), not different from the control value of 71% (data not shown). We sought to determine the degree of inhibition produced by 300 μM or 150 μM SR-95531 (5 cells each) on delayed release events recorded in 8 mM Sr^{2+} following train stimuli, but found that the antagonist reduced the detection rate of these events too severely. In those experiments, the amplitude of low-frequency evoked IPSCs were reduced by 88±3% by 300 μM and 77±4% by 150 μM SR-95531, and thus it is not surprising that most quantal events would be undetectable. Given that the degree of block is lowest for evoked responses in the presence of Ca^{2+}, we conclude that multivesicular release must determine the peak amplitude of evoked IPSCs.

To further explore the ability of the SR-95531 to interact with receptors on the time frame of transmitter release and clearance, we examined the response to stimulus trains. During trains, the IPSC amplitude (foot-to-peak) of later events grew smaller, presumably as a result of synaptic depression and/or receptor saturation. If the GlyRs are progressively saturated by accumulating transmitter, the relative magnitude of this decline in amplitude should be reduced by SR-95531. The first IPSCs in trains recorded in control and SR-95531 were normalized so that the relative amplitude of the later IPSCs in the train could be compared to the first IPSC. The ratio of the mean of the last five events to the first IPSC ($IPSC_{5\text{-}10}$/$IPSC_1$) in controls was significantly less than in SR-95531 (paired t-test, P=0.0015 n=10, Fig 4c,d), indicating that receptor saturation increases during high-frequency IPSCs.

If the concentration of glycine falls gradually, then the low-affinity antagonist should become progressively more effective in preventing rebinding of glycine to its receptor. A consequence of this effect would be an acceleration of the decay of synaptic current. Supporting this hypothesis, the decay of IPSCs during single and train of stimulation was accelerated by SR-95531 (Fig 5). Upon application of SR-95531 during single stimulation,

the mean weighted decay time significantly decreased from 23±3 to 17±2 ms (25±5% decrease; n=9; P=0.003, paired t-test; Fig. 5a,b,e). During train stimulation, the weighted decay time decreased significantly from 58±8 to 47±7 ms (21±3% decrease; n=10; P=0.0001, paired t-test). As a control, we examined the effect of a submaximal concentration of strychnine, a high-affinity antagonist. Strychnine (200 nM) had no effect on the synaptic decay time, despite blocking the IPSC to a nearly identical level (Fig 5c,d,f). Thus, we conclude that multivesicular release of glycine leads to a delay in the clearance of transmitter from the synaptic cleft and a prolonged IPSC decay.

Predictions of kinetic modeling

Our data suggest that the lifetime of transmitter in the synaptic cleft can change with stimulus condition, and thus regulate the decay time of IPSCs. To explore what transmitter timecourses are consistent with these results, we drove a kinetic model of GlyRs with different glycine concentration transients. We adopted a model from Burzomato et al. 18, based on cell-attached single-channel recordings, and modified it to include desensitization and competitive antagonism (see Supplemental Material for a complete description of the model and its results). This model, as well as results from previous studies, highlight features that suggest a unique ability of the GlyR to respond to changes in transmitter transients with changes in synaptic decay time 5, 19, 38-41, most notably the presence of multiple binding sites and associated open states with distinct burst times, as well as comparatively little desensitization. Transmitter transients at single synaptic sites are typically quite rapid. Although peak levels of transmitter reach the mM range, diffusion models predict that the majority of transmitter is cleared rapidly, and can be approximated with a major exponential component of less than 100 μsec, and a slower component of a few ms 42. We explored the behavior of the model with a peak of 6 mM and fast decay of 80 μs, followed by a slower component with a peak of 15 μM and a 5-ms decay time (see Supplemental Materials for more extensive testing of parameters). This resulted in an IPSC with an 8.3 ms exponential decay time (Fig. 6a), similar to the decay of asynchronous quantal currents (Fig 2c,d), but faster than typical evoked events (Fig 2b). Indeed, significant slowing of the IPSC decay (without concomitant slowing of the rise time) could only be obtained by lengthening dramatically the duration of the smaller, second component of decay. This immediately implies that rebinding of glycine to the receptor must occur during the IPSC decay. Moreover, given that very slow decay components like these are inconsistent with diffusion from a single synaptic site 42, the slow decay must reflect transmitter pooling from many synaptic sites.

IPSC decays as slow as those observed experimentally for single stimuli in 2 mM Ca^{2+} required a slow component of at least 60 ms (Fig. 6a, Supplemental Fig S3). During train stimuli, this slow component summated, and predicted a marked slowing of the simulated IPSC to an extent similar to that seen experimentally (Fig. 6b) – such slowing of train responses was not seen when the 60-ms glycine decay was reduced back to 5 ms (Fig S4). The IPSC decay could also be markedly affected by scaling the amplitude of the glycine waveform 0.5-2 fold, to mimic the effects of multivesicular release (Fig. 6c); however this effect required the additional presence of pooling (see Fig S6). Finally, we mimicked the effect of the weak antagonist SR-95531, using the parameters of Beato et al. 36 (see

Supplemental Materials). At 300 μM SR-95531, the model predicted (Fig. 6d) that the IPSC would be reduced to 34% of control (compared to 30% seen experimentally) and that the weighted decay time after single shocks or 100 Hz trains would be reduced by 28% and 29% (compared to 27% and 28% seen experimentally). The magnitude of the effect of the antagonist on decay time could only be reproduced if a very slow phase of clearance was assumed (Fig S5, S6). When the antagonist simulation was retested using a transient with cleft glycine concentration scaled down by half (simulating reduced multivesicular release, as in Fig. 6c) the peak response was reduced to 11% of control, as compared to 14% measured in 1 mM Ca^{2+} (Fig. 3b, S6). As expected, the simulation of SR-95531 also predicted that receptor saturation in trains would be reduced, a result entirely dependent on the presence of slow glycine clearance (Fig S4). This modeling approach is limited by a lack of information of the spatial distribution of synapses and their release probabilities. Biological variation in these parameters could explain why IPSC decays vary so widely in different cells. Nevertheless, it is compelling that the IPSC waveforms we have observed under diverse experimental conditions can be accounted for quantitatively by assuming use-dependent pooling of glycine around granule cells.

Slowing of the decay phase increases effectiveness of inhibition

We explored the physiological significance of the variation in decay time by delivering single and repetitive IPSPs and determining how long the IPSPs were able to delay resumption of action potential firing. AMPA, NMDA and $GABA_A$ receptor blockers were added to the extracellular solution to isolate glycinergic IPSPs. A continuous depolarizing current injection of 5-10 pA elicited steady action potentials. In response to presynaptic stimuli, IPSPs hyperpolarized the cells and abruptly halted firing (Fig. 7a). Upon a single IPSP, spikes were inhibited for 192±66 ms (latency from stimulus artifact to first spike; n=8). By contrast, upon a train of IPSPs (10 stimuli) the inhibition *after* the last stimulus was prolonged by over 100 ms (Fig 7a-c; 326±83 ms from last stimulus artifact to resumption of spikes; 91±19% increase; P=0.0015; n=8). While the extent of the delay varied widely among cells (Fig. 7c), the increase in delay was seen in every case, and larger IPSPs tended to produce longer delays (Fig 7d). This effect is not due to recruitment of intrinsic currents by the IPSP, such as A-type K^+ currents, as direct hyperpolarizing current injections of different durations produced spike delays of less than 40 ms, much briefer than that seen with IPSPs (Fig 7e-h). Moreover, this difference in decay time between single and train IPSPs is not due to differences in peak synaptic conductance, as demonstrated by examining the duration of spike inhibition with IPSGs of identical duration but different amplitude (Fig S7). Thus, the changes we have observed in the decay of synaptic currents results in comparable changes in the lifetime of inhibition.

Spillover from glycinergic boutons

Given the magnitude of the spillover component suggested by our data, we asked whether, in principle, the density of glycinergic terminals near granule cells would predict such a pool of extrasynaptic transmitter. Glycinergic cells were identified in mice expressing GFP driven by the promoter for GlyT2 (see Supplemental Materials). Tissue sections were then labeled with an antibody to the GABA/glycine vesicular transporter VIAAT, and convergence of the two labels were used to identify glycinergic boutons (see Methods for

complete description of labeling and analysis). This approach proved preferable to labeling with GlyT2 antibodies, as we found both synaptic and non-synaptic structures labeled with that a GlyT2 antibody. In the same tissue slice, 2-3 granule cells were labeled by electroporation of rhodamine-dextran conjugate (Fig 8A-F).

Confocal sections were made of a 10×10×2 μm volume containing a granule cell dendrite, and a thresholding procedure was used to resolve labeled objects (see Methods). The number of nerve terminals/region was then calculated by dividing the total volume of GFP/VIAAT positive objects by the median volume of these objects. This approach gave an average terminal density of 0.059±0.021 terminals/μm^3 (6 filled granule cells, 15 regions analyzed, range 0.027-0.1/μm^3). We then simulated diffusion from an array of 512 terminals (sources) arranged uniformly at different densities within the measured range (Fig 8G for 0.08/μm^3) and estimated the concentration at a point in the center of the volume (black spot in Fig 8G) over time following exocytosis from the individual sites (ref. 42; see Methods for equation parameters). Summing contributions from all sources gave a transient that rose to 10 μM and decayed over several hundred ms, which should have produced a small, slow receptor response (Fig 8H). We then drove our kinetic model of the receptor with a transient representing the sum of the slow spillover component and the large, rapidly decaying transient expected for localized transmission (fast decay phase 80 μs, slow phase 5 ms), as described above. The kinetic model yielded a waveform remarkably similar in decay time to recorded IPSCs (Fig 8I). Thus, in principle, glycine spillover adding to local transmission could account for the slow IPSCs in DCN granule cells.

Discussion

The decay of a synaptic response is generally viewed as reflecting the intrinsic gating kinetics of receptors, when transmitter clearance is rapid, or transmitter rebinding and reactivation of receptors when clearance is slow. Clearance of transmitter is delayed when transmitter pools in or around the synaptic cleft. Some glutamatergic synapses are suited to transmitter pooling by virtue of a high density of synaptic sites 43 or an especially broad synaptic cleft 8. However in these cases, the effects of pooling are strongly supra-linear, in the sense that small increases in stimulus number produces large enhancement and prolongation of synaptic current and a parallel increase in spiking. Such nonlinearity is optimal for amplification of excitatory signals but not well-suited for transmitting graded changes in the level of excitation over a wide range. Our analysis of inhibitory glycinergic transmission reveals an effect on decay more linearly related to stimulus number and to the number of quanta released per stimulus. We also observed a very wide range of decay times among cells (~10-fold), suggesting that, besides regulating decay time in an activity-dependent manner, different neurons may have their own set-points for pooling, perhaps determined by different densities of nerve terminals. Such a dense glycinergic neuropil is consistent with our analysis and with previous anatomical studies 44.

This study revealed that multivesicular release contributes to determining the amplitude of the IPSC. Distinguishing relative roles for multivesicular release and spillover from adjacent synapses is challenging 32, 45. We concluded that multivesicular release determines peak IPSC amplitude because 1) the effect of the low-affinity antagonist SR-95531 on peak

current was Ca^{2+}-dependent, 2) glycine uptake blockers did not change the effectiveness of the antagonist, 3) nor alter the peak amplitude of the IPSC, and 4) larger IPSCs did not rise more slowly than small IPSCs. By contrast, pooling is likely to set the decay time because 1) increasing stimulus strength recruited additional fibers and slowed the decay time, 2) increasing stimulus number or frequency slowed the decay time (such slowing was seen at intervals as slow as 50 ms, suggesting that pooling must accumulate transmitter at least over this time frame) 3) SR-95531 shortened the decay time, 4) kinetic models indicating that GlyRs do not generate fast-rising, slowly-decaying IPSCs without a considerable delay in the clearance of transmitter, and 5) the density of glycinergic terminals surrounding granule cells would be expected to generate a significant spillover component.

Glycinergic synapses vary widely in their decay kinetics. Decay times are extremely fast in most glycinergic synapses of the spinal cord and brainstem, where they presumably reflect solely the biophysical properties of the GlyR. The deactivation time of GlyRs following removal of glycine can be as fast as 4-6 ms 5, 22, 39, although this estimate can be significantly affected by the duration of agonist exposure 19, 40. As the decay time of glycinergic IPSCs in brainstem and spinal cord are often in the range of 4-6 ms, it is generally thought that deactivation determines the synaptic decay and that glycine clearance must be quite fast. A recent study in spinal cord showed that glycine reached a peak of about 3 mM and cleared the synapse in about 1 ms, resulting in a fast IPSC decay 20. Accordingly, in that study, SR-95531 had no effect on the IPSC decay time. For some cases in the auditory system, glycinergic IPSC decays can be even faster still 19, 28, due to extremely rapid transmitter removal and the action of coreleased GABA on the gating of GlyRs 19. In all of these cases, it is likely that fast inhibition allows for effective temporal convergence of signals within a neural circuit.

By contrast, in thalamus, retina, and cerebellum, the decay of glycinergic IPSCs, or deactivation of GlyR, can range from 10-40 ms or more 46-48. To account for the slow decays seen in auditory granule cells, we initially suspected the expression of a different subtype of synaptic GlyR, and indeed α2 receptors have been associated with slower gating in some cases 48. However this is unlikely in granule cells, for several reasons. α1, the most common subsynaptic α subunit, is detected in granule cells while α2 is not 49. More importantly, the effect of subunit composition would not likely be sensitive to quantal content or stimulus intensity, number or frequency; indeed, for quantal currents recorded in Sr^{2+}, synaptic decays were similar to those reported at more classical inhibitory synapses on motor neurons 22. Interestingly, the decay time of glycinergic currents in granule cells are similar to those of cerebellar Golgi cells, with time constants up to 40 ms 46, suggesting that the mechanism we have described may be common to cerebellum-like systems.

The amount of pooled transmitter was graded with the number of axons activated or the number/frequency of stimuli, resulting in progressively slower decays. At the same time, the rise time of IPSCs was constant, consistent with a transmitter timecourse like that used in our model: a rapid and local transient followed by a smaller, slow decay. Trains of slow IPSCs led to steady plateau currents 27 and should therefore produce DC-like changes in the level of inhibition. A similar plateau inhibition with slow decay times has been described at subtypes of GABAergic synapses, but utilizing a very different mechanism 16. There,

asynchronous release develops during the stimulus train, smoothing out the current between stimuli and dramatically slowing the current decay time. Glycinergic synapses do not appear as susceptible to induction of asynchronous release, even at high stimulus rates 50. Although transmitter pooling permits these synapses to adjust decay times in an activity dependent manner, a key difference from the GABAergic synapses is that asynchronous release is local to each synapse, while pooling would be expected to have effects over larger regions of the cell or even on neighboring cells.

Methods

Coronal brainstem slices containing the DCN (200 μm) were prepared from Wistar rats (postnatal day 14 (P14) - P25). The care and use of animals was approved by the Institutional Animal Care and Use Committee of OHSU. Animals were anesthetized before decapitation and brains were removed in warm (35°C) ACSF composed of (in mM) 125 NaCl, 25 glucose, 2 KCl, 1 $MgCl_2$, 2 $CaCl_2$, 1.25 NaH_2PO_4, 26 $NaHCO_3$, 0.4 ascorbic acid, 2 Na-pyruvate, 3 myo-inositol, bubbled with 5% CO_2-95% O_2 (pH 7.4). Slices were then incubated for 25 min in warm ACSF. Recordings were made at 33−35 °C, typically within 4 h of slicing. Neurons were visualized with differential interference contrast microscopy using a 40x water-immersion objective.

For current clamp, the pipette solution contained (in mM) 145 K-gluconate, 1 $MgCl_2$, 10 HEPES, 0.2 EGTA, 4 ATP, 0.3 GTP and pH adjusted to 7.3 with KOH. Voltage signals were corrected off-line for a 11-mV junction potential. For voltage clamp, the pipette solution contained (in mM) 110 CsCl, 40 HEPES, 2 NaCl, 5 EGTA, 4 Mg-ATP, 0.3 Na-GTP, and pH adjusted to 7.3 with CsOH. For asynchronous release experiments, 8 mM $SrCl_2$ replaced $CaCl_2$. One set of voltage-clamp experiments testing the effect of low [Cl] on IPSC decay used a pipette solution containing (mM) 108 $CsMeSO_3$, 5 CsCl, 1 $MgCl_2$, 4 Mg-ATP, 0.4 Tris-ATP, 14 Tris-phosphocreatine, 5 EGTA, 10 HEPES, 3 QX-314, pHs to 7.3 with CsOH. A 100-200-μs, 5-50-isolated V pulse delivered via an electrode filled with extracellular solution was used to stimulate inhibitory axons. The placement and the stimulus intensity were optimized to obtain the most stable responses. Glycinergic IPSCs were recorded with 10 μM DNQX, 50 μM AP5, 10 μM SR 95531, and 10 μM picrotoxin (in some experiments) at a holding potential of −70 mV. With this solution, all synaptic responses could be completely blocked by addition of strychnine (0.5 μM; n=5) (Fig.1c). Synaptic currents were evoked by extracellular stimulation with a bipolar glass electrode placed ∼30-40 μm away from the granule cell. The currents were recorded with an Axopatch 200B amplifier and Clampex software (Molecular Devices).

Evoked IPSCs were analyzed in Clampfit 9.2 (Molecular Devices). Aligned IPSCs were averaged, and the decays were fit by single or double exponential functions (based on the improvement of the summed square error): $D(t) = A_{FAST} \times e^{(-t/\tau FAST)} + A_{SLOW} \times e^{(-t/\tau SLOW)}$, where $D(t)$ is the decay of the mIPSC as a function of time (t); A_{FAST} and A_{SLOW} are constants; and τ_{FAST} and τ_{SLOW} are fast and slow decay time constants, respectively. In some cases, adding the second exponential component did not significantly decrease the SSE, and so A_{SLOW} was set at to 0. The weighted decay time constant was calculated as $\tau_{wd}=(A_{FAST}\times\tau_{fast} + A_{SLOW}\times\tau_{slow})/(A_{FAST}+A_{SLOW})$. Percentage of fast component was

calculated as% Fast=(A_{fast}/(A_{fast} + A_{slow}))×100. For instances in which the decay had more linear components, an equivalent exponential decay time was determined by normalizing the peak to 1 and integrating the entire decay phase. Results are expressed as mean±s.e.m., and the significance was determined using Student's paired *t*-test (significance indicated by $P < 0.05$, except as indicated).

Kinetic simulations, immunohistochemistry, conductance clamp experiments and diffusion modeling

see Supplemental Materials.

Chemicals

DL-AP5, DNQX, NBQX, and SR95531 were obtained from Ascent Scientific. E4CPG, CPPG, CGP-55845 Tocris. ORG-25543 a gift of Hardy Sundaram, Organon Biosciences. All other chemicals were from Sigma. Drugs were dissolved in extracellular solution. In some cases, drugs were first dissolved in DMSO (final DMSO concentration of 0.01%).

Supplementary Material

Refer to Web version on PubMed Central for supplementary material.

Acknowledgements

We thank Drs. Hai Huang, Craig E. Jahr, and Michael E. Roberts for comments on the manuscript and Dr. Hardy Sundaram for the gift of ORG-25543. This work was supported by NS028901.

REFERENCES

1. Katz B, Miledi R. The binding of acetylcholine to receptors and its removal from the synaptic cleft. J Physiol. 1973; 231:549–574. [PubMed: 4361216]
2. Barrett EF, Stevens CF. The kinetics of transmitter release at the frog neuromuscular junction. J Physiol. 1972; 227:691–708. [PubMed: 4405553]
3. Barbour B, Keller BU, Llano I, Marty A. Prolonged presence of glutamate during excitatory synaptic transmission to cerebellar Purkinje cells. Neuron. 1994; 12:1331–1343. [PubMed: 7912092]
4. Jones MV, Westbrook GL. Desensitized states prolong GABAA channel responses to brief agonist pulses. Neuron. 1995; 15:181–191. [PubMed: 7542462]
5. Legendre P. A reluctant gating mode of glycine receptor channels determines the time course of inhibitory miniature synaptic events in zebrafish hindbrain neurons. J Neurosci. 1998; 18:2856–2870. [PubMed: 9526003]
6. Takahashi T, Momiyama A, Hirai K, Hishinuma F, Akagi H. Functional correlation of fetal and adult forms of glycine receptors with developmental changes in inhibitory synaptic receptor channels. Neuron. 1992; 9:1155–1161. [PubMed: 1281418]
7. Otis T, Zhang S, Trussell LO. Direct measurement of AMPA receptor desensitization induced by glutamatergic synaptic transmission. J Neurosci. 1996; 16:7496–7504. [PubMed: 8922405]
8. Kinney GA, Overstreet LS, Slater NT. Prolonged physiological entrapment of glutamate in the synaptic cleft of cerebellar unipolar brush cells. J Neurophysiol. 1997; 78:1320–1333. [PubMed: 9310423]
9. Otis TS, Wu YC, Trussell LO. Delayed clearance of transmitter and the role of glutamate transporters at synapses with multiple release sites. J Neurosci. 1996; 16:1634–1644. [PubMed: 8774432]

10. Silver RA, Cull-Candy SG, Takahashi T. Non-NMDA glutamate receptor occupancy and open probability at a rat cerebellar synapse with single and multiple release sites. J Physiol. 1996; 494(Pt 1):231–250. [PubMed: 8814618]
11. Kondo S, Marty A. Synaptic currents at individual connections among stellate cells in rat cerebellar slices. J Physiol. 1998; 509(Pt 1):221–232. [PubMed: 9547395]
12. Biro AA, Holderith NB, Nusser Z. Release probability-dependent scaling of the postsynaptic responses at single hippocampal GABAergic synapses. J Neurosci. 2006; 26:12487–12496. [PubMed: 17135411]
13. Cathala L, Holderith NB, Nusser Z, DiGregorio DA, Cull-Candy SG. Changes in synaptic structure underlie the developmental speeding of AMPA receptor-mediated EPSCs. Nat Neurosci. 2005; 8:1310–1318. [PubMed: 16172604]
14. Isaacson JS, Solis JM, Nicoll RA. Local and diffuse synaptic actions of GABA in the hippocampus. Neuron. 1993; 10:165–175. [PubMed: 7679913]
15. Banks MI, Li TB, Pearce RA. The synaptic basis of GABAA,slow. J Neurosci. 1998; 18:1305–1317. [PubMed: 9454840]
16. Lu T, Trussell LO. Inhibitory transmission mediated by asynchronous transmitter release. Neuron. 2000; 26:683–694. [PubMed: 10896163]
17. Legendre P. The glycinergic inhibitory synapse. Cell Mol Life Sci. 2001; 58:760–793. [PubMed: 11437237]
18. Burzomato V, Beato M, Groot-Kormelink PJ, Colquhoun D, Sivilotti LG. Single-channel behavior of heteromeric alpha1beta glycine receptors: an attempt to detect a conformational change before the channel opens. J Neurosci. 2004; 24:10924–10940. [PubMed: 15574743]
19. Lu T, Rubio ME, Trussell LO. Glycinergic transmission shaped by the co-release of GABA in a mammalian auditory synapse. Neuron. 2008; 57:524–535. [PubMed: 18304482]
20. Beato M. The time course of transmitter at glycinergic synapses onto motoneurons. J Neurosci. 2008; 28:7412–7425. [PubMed: 18632945]
21. Brand A, Behrend O, Marquardt T, McAlpine D, Grothe B. Precise inhibition is essential for microsecond interaural time difference coding. Nature. 2002; 417:543–547. [PubMed: 12037566]
22. Singer JH, Berger AJ. Contribution of single-channel properties to the time course and amplitude variance of quantal glycine currents recorded in rat motoneurons. J Neurophysiol. 1999; 81:1608–1616. [PubMed: 10200197]
23. Harty TP, Manis PB. Kinetic analysis of glycine receptor currents in ventral cochlear nucleus. J Neurophysiol. 1998; 79:1891–1901. [PubMed: 9535956]
24. Mager S, et al. Steady states, charge movements, and rates for a cloned GABA transporter expressed in Xenopus oocytes. Neuron. 1993; 10:177–188. [PubMed: 7679914]
25. Wadiche JI, Arriza JL, Amara SG, Kavanaugh MP. Kinetics of a human glutamate transporter. Neuron. 1995; 14:1019–1027. [PubMed: 7748550]
26. Oertel D, Young ED. What's a cerebellar circuit doing in the auditory system? Trends Neurosci. 2004; 27:104–110. [PubMed: 15102490]
27. Balakrishnan V, Trussell LO. Synaptic inputs to granule cells of the dorsal cochlear nucleus. J Neurophysiol. 2008; 99:208–219. [PubMed: 17959739]
28. Awatramani GB, Turecek R, Trussell LO. Inhibitory control at a synaptic relay. J Neurosci. 2004; 24:2643–2647. [PubMed: 15028756]
29. Magnusson AK, Kapfer C, Grothe B, Koch U. Maturation of glycinergic inhibition in the gerbil medial superior olive after hearing onset. J Physiol. 2005; 568:497–512. [PubMed: 16096336]
30. Silver RA, Traynelis SF, Cull-Candy SG. Rapid-time-course miniature and evoked excitatory currents at cerebellar synapses in situ. Nature. 1992; 355:163–166. [PubMed: 1370344]
31. Pitt SJ, Sivilotti LG, Beato M. High Intracellular Chloride Slows the Decay of Glycinergic Currents. Journal of Neuroscience. 2008; 25:11454–11467. [PubMed: 18987182]
32. Christie JM, Jahr CE. Multivesicular release at Schaffer collateral-CA1 hippocampal synapses. J Neurosci. 2006; 26:210–216. [PubMed: 16399689]
33. Tong G, Jahr CE. Block of glutamate transporters potentiates postsynaptic excitation. Neuron. 1994; 13:1195–1203. [PubMed: 7946356]

34. Atkinson BN, et al. ALX 5407: a potent, selective inhibitor of the hGlyT1 glycine transporter. Mol Pharmacol. 2001; 60:1414–1420. [PubMed: 11723250]
35. Whitehead KJ, et al. Positive N-methyl-D-aspartate receptor modulation by selective glycine transporter-1 inhibition in the rat dorsal spinal cord in vivo. Neuroscience. 2004; 126:381–390. [PubMed: 15207356]
36. Beato M, Burzomato V, Sivilotti LG. The kinetics of inhibition of rat recombinant heteromeric alpha1beta glycine receptors by the low-affinity antagonist SR-95531. J Physiol. 2007; 580:171–179. [PubMed: 17218350]
37. Wang P, Slaughter MM. Effects of GABA receptor antagonists on retinal glycine receptors and on homomeric glycine receptor alpha subunits. J Neurophysiol. 2005; 93:3120–3126. [PubMed: 15728760]
38. Fucile S, de Saint Jan D, David-Watine B, Korn H, Bregestovski P. Comparison of glycine and GABA actions on the zebrafish homomeric glycine receptor. J Physiol. 1999; 517(Pt 2):369–383. [PubMed: 10332088]
39. Gentet LJ, Clements JD. Binding site stoichiometry and the effects of phosphorylation on human alpha1 homomeric glycine receptors. J Physiol. 2002; 544:97–106. [PubMed: 12356883]
40. Mohammadi B, et al. Kinetic analysis of recombinant mammalian alpha(1) and alpha(1)beta glycine receptor channels. Eur Biophys J. 2003; 32:529–536. [PubMed: 14551753]
41. Twyman RE, Macdonald RL. Kinetic properties of the glycine receptor main- and sub-conductance states of mouse spinal cord neurones in culture. J Physiol. 1991; 435:303–331. [PubMed: 1722820]
42. Barbour B, Hausser M. Intersynaptic diffusion of neurotransmitter. Trends Neurosci. 1997; 20:377–384. [PubMed: 9292962]
43. Carter AG, Regehr WG. Prolonged synaptic currents and glutamate spillover at the parallel fiber to stellate cell synapse. J Neurosci. 2000; 20:4423–4434. [PubMed: 10844011]
44. Alibardi L. Ultrastructural distribution of glycinergic and GABAergic neurons and axon terminals in the rat dorsal cochlear nucleus, with emphasis on granule cell areas. J Anat. 2003; 203:31–56. [PubMed: 12892405]
45. Wadiche JI, Jahr CE. Multivesicular release at climbing fiber-Purkinje cell synapses. Neuron. 2001; 32:301–313. [PubMed: 11683999]
46. Dumoulin A, Triller A, Dieudonne S. IPSC kinetics at identified GABAergic and mixed GABAergic and glycinergic synapses onto cerebellar Golgi cells. J Neurosci. 2001; 21:6045–6057. [PubMed: 11487628]
47. Kraushaar U, Backus KH. Characterization of GABA(A) and glycine receptors in neurons of the developing rat inferior colliculus. Pflugers Arch. 2002; 445:279–288. [PubMed: 12457249]
48. Veruki ML, Gill SB, Hartveit E. Spontaneous IPSCs and glycine receptors with slow kinetics in wide-field amacrine cells in the mature rat retina. J Physiol. 2007; 581:203–219. [PubMed: 17331993]
49. Piechotta K, Weth F, Harvey RJ, Friauf E. Localization of rat glycine receptor alpha1 and alpha2 subunit transcripts in the developing auditory brainstem. J Comp Neurol. 2001; 438:336–352. [PubMed: 11550176]
50. Awatramani GB, Turecek R, Trussell LO. Staggered development of GABAergic and glycinergic transmission in the MNTB. J Neurophysiol. 2005; 93:819–828. [PubMed: 15456797]

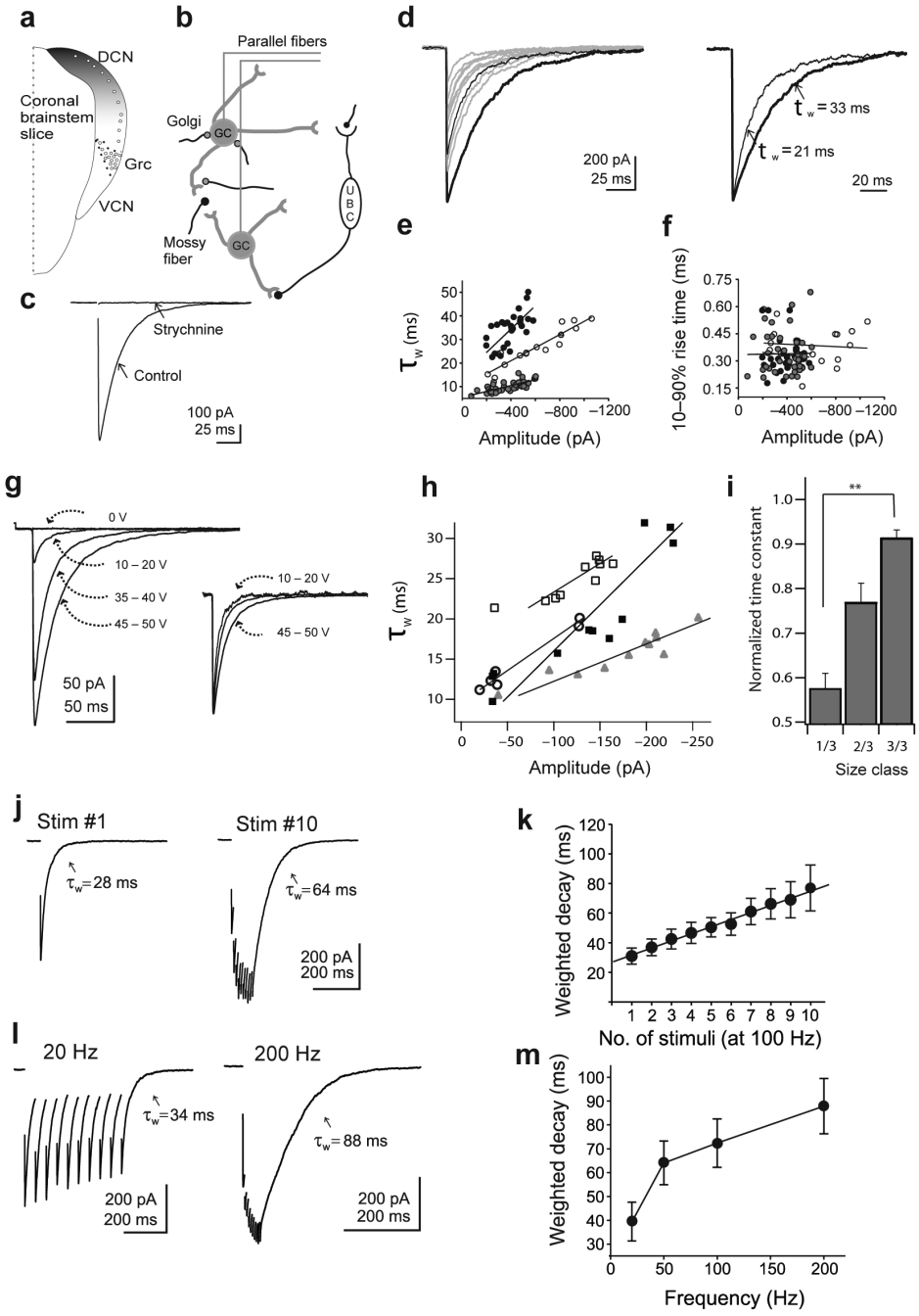

Figure 1. Granule cells in the dorsal cochlear nucleus (DCN) and their glycinergic postsynaptic currents

(a) Schematic representation of the cochlear nucleus in a coronal brainstem slice, showing the distribution of granule cells (circles) in the DCN and the granule cell region (Grc). (b) Synaptic inputs to granule cells. Granule cells receive excitatory inputs through mossy fibers and the unipolar brush cells (UBC). Inhibitory inputs are assumed to be from the Golgi/stellate neurons. (c) Averaged glycinergic IPSC from a granule cell under control conditions and in 0.5 μM strychnine application. (d) Example traces of glycinergic IPSCs upon synaptic stimulation. Two sample IPSCs of different size are shown in thick and thin black lines. On

the right, these IPSCs were normalized and their corresponding weighted decay times are shown. (e) The weighted decay constants of the IPSCs positively correlated with the amplitude. Plot show the values from three cells and their corresponding regression line. The linear fits in the three plots have r=0.92, 0.68 and 0.76 with P<0.0001 for all. (f) IPSC rise times and amplitudes had no correlation. The values from three cells, plotted as rise time and amplitude. Linear fits are insignificant for all cells. (g) Example IPSCs evoked at various voltages. The inset shows the traces normalized, revealing that responses to smaller stimuli decay more quickly. (h) Correlation of amplitude and weighted decay as stimulus strength was changed in four neurons. Correlation coefficients were 0.88, 0.91, 0.93, 0.99 (P<0.002). (i) Normalized amplitudes of responses were grouped into upper, middle, and lower thirds of the population, and their corresponding decay times averaged (9 cells, 15-36 measurements/ category, P<0.002 between categories). (j) Examples of glycinergic IPSCs evoked with one and ten stimuli (10 ms interval). (k) Weighted decay times of the IPSCs against number of stimuli (100 Hz) from five cells. (l) Ten IPSCs delivered at 20 Hz and 200 Hz. (m) Weighted decay times from 7 cells at different frequencies. Comparison of decay times at different frequencies: 20-50 Hz; P<0.01, 50-100 Hz; P<0.05, 100-200 Hz; P < 0.001). Error bars are ±SEM.

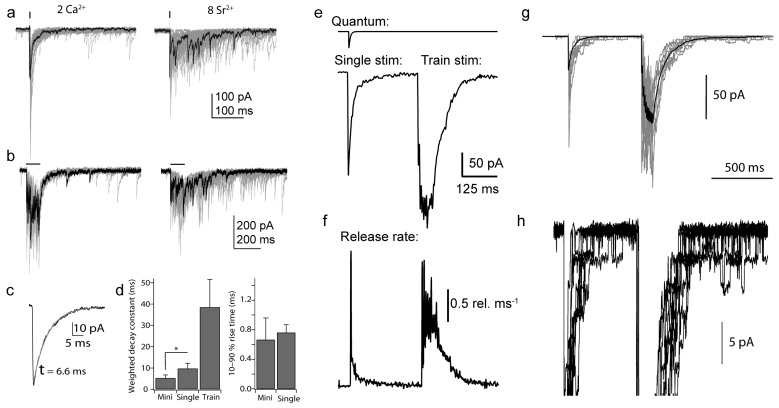

Figure 2. Asynchronous release

(a) Evoked responses in 2 mM Ca^{2+} and 8 mM Sr^{2+}. (b) Response to 10 stimuli (100 Hz) in 2 mM Ca^{2+} and 8 mM Sr^{2+}. In all cases asynchronous release events are clearly visible. Black trace highlights one of 25-51 in each panel. All data shown are from one cell. (c) Averaged delayed release IPSC from data shown in a-b. (d) Decay time constant for delayed release events ('mini'), and response to single stimuli or trains of 10 shocks at 100 Hz. Rise time of quanta and evoked responses were not significantly different. Asterisk: $P<0.01$. n=5 cells. (e) Simulated quantal current ($34\ pA^{*} -(1-\exp^{-t/0.4ms})^{2}*(\exp^{-t/8ms})$) and an unaveraged trace showing response to a single stimulus and to a train of 10 stimuli delivered at 100 Hz. (f) Deconvolved release rate from traces in panel e. (g) Ten low-noise traces from one cell showing response to single and train of 10 stimuli. Average of 64 such traces is superimposed in black (decay times were 38 ms and 89 ms for single and train response). (h) Same sweeps as in panel g, shown at higher gain to illustrate single-channel currents. Error bars are ±SEM.

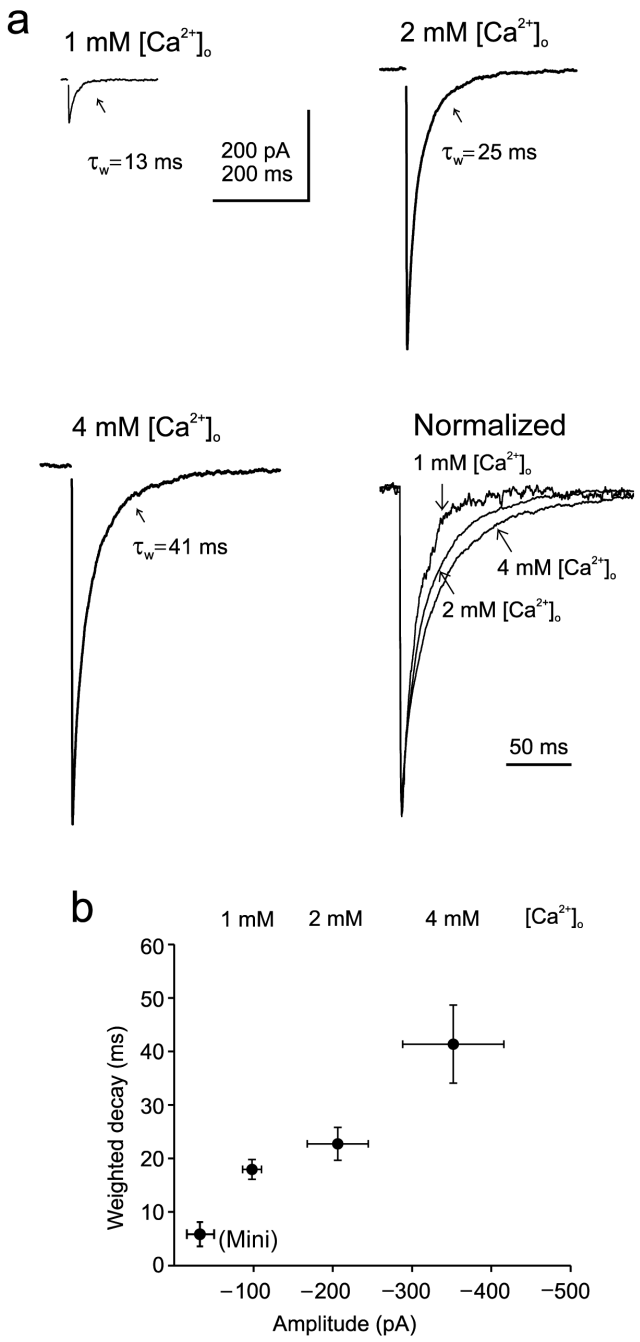

Figure 3. Increasing release probability slows IPSC decay time

(a) Averaged glycinergic IPSCs recorded in different bath Ca^{2+} concentrations. Corresponding weighted decay constants are also shown. (b) Relation between amplitude and decay time in three Ca^{2+} concentrations, as indicated (n=5 cells). In lower left are the mean amplitude and decay time for delayed release events (‘mini’) for 5 cells. Error bars are ±SEM.

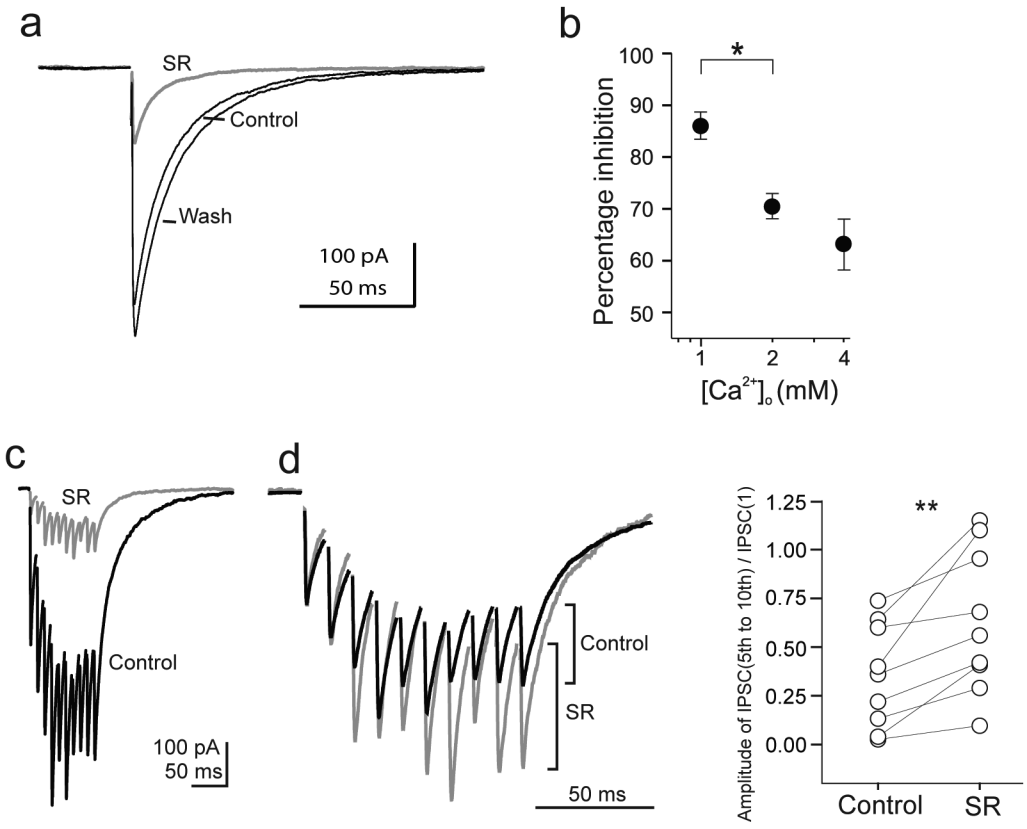

Figure 4. Probing multivesicular release and receptor saturation using a weak antagonist of GlyRs, SR-95531

(a) Block of IPSC by 300 μM SR-95531 (SR). (b) Percent reduction in IPSC amplitude by 300 μM SR-95531 in different Ca^{2+} concentrations. 4-9 cells per point. Values for 1 and 2 mM Ca^{2+} are significantly different ($P<0.05$). (c) SR-95531 inhibition of responses to a train of 10 IPSCs at 100 Hz. (d) Traces in (c) were normalized to the first IPSC in the train. Amplitudes of later IPSCs in the train were measured from the foot to peak, as indicated. Traces are averages of 20 trials. (e) Summary of the peak amplitudes of the last five IPSCs in a train in control and in the presence of SR-95531 for 10 experiments in which the amplitudes were normalized to first IPSC. A comparison of the responses in control and SR-95531 revealed that there was a significant increase in the relative amplitude of later IPSCs ($P < 0.0015$, paired t-test) indicating that SR-95531 relieves saturation during high-frequency trains. Error bars are ±SEM.

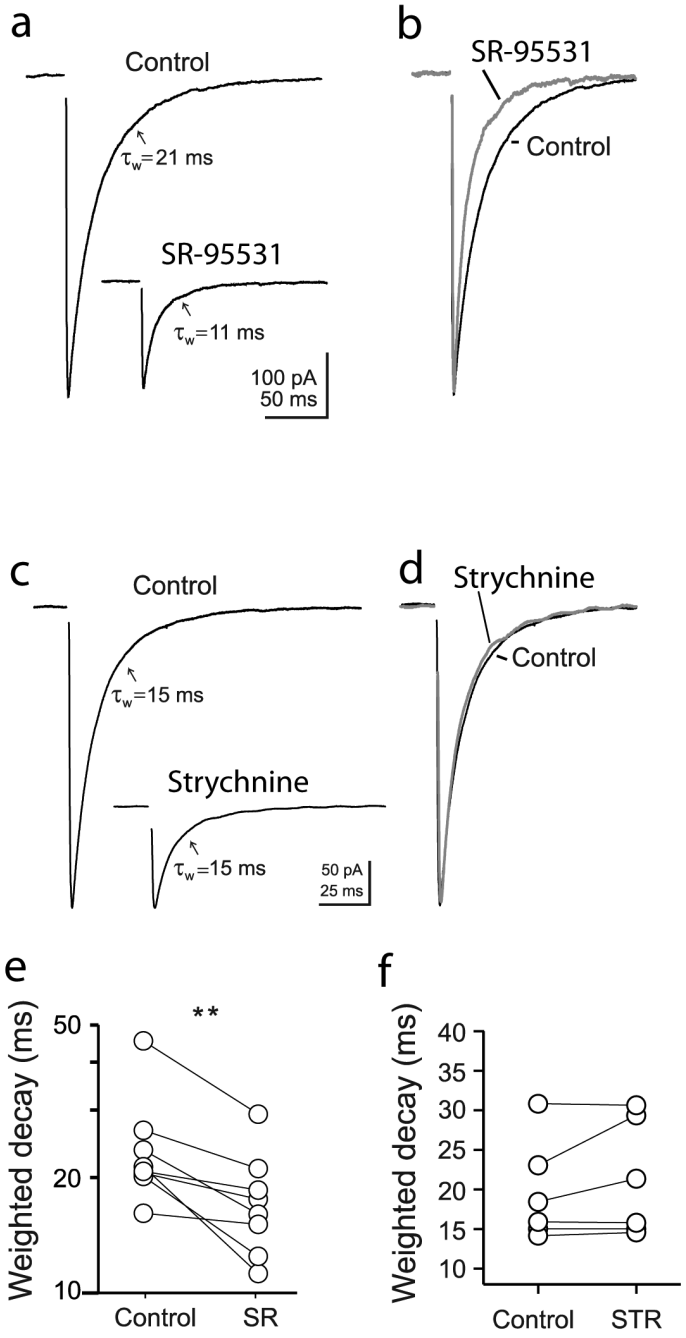

Figure 5. SR-95531 accelerates the decay of IPSCs

(a) Example of averaged and (b) normalized glycinergic IPSCs upon single stimulation in control and in the presence of 300 μM SR-95531. (c) Example of averaged and normalized (d) traces with and without 200 nM strychnine. (e,f) Effect of SR-95531 (SR) and strychnine (STR) on weighted decay time. Paired t-tests were significant only for the SR-95531 trials ($P<0.003$).

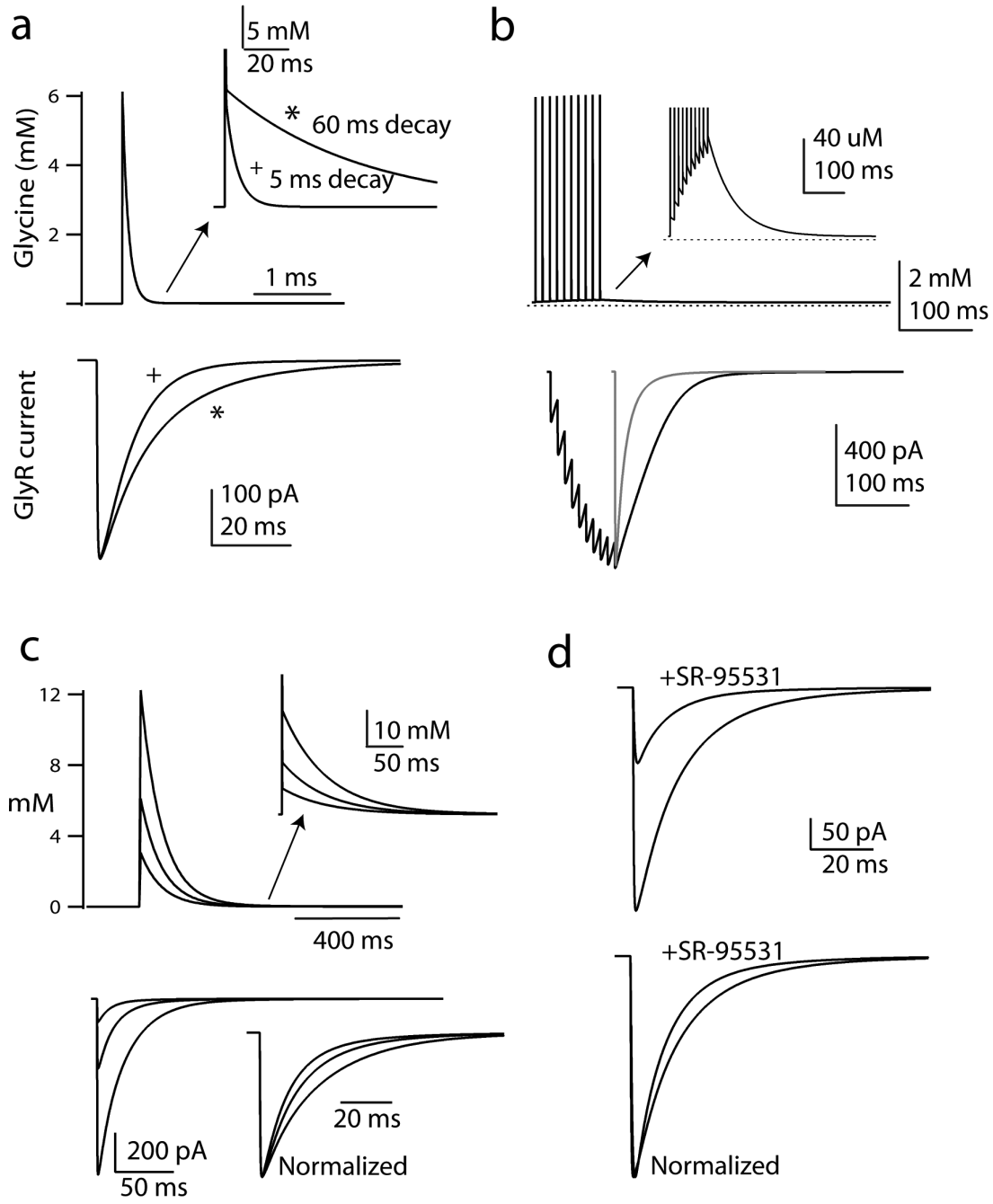

Figure 6. Simulation of IPSCs

(a) The glycine transient had a peak of 6 mM and fast decay constant of 80 μs. Inset shows the same traces but different scale to illustrate two slow decay constants, of 5 ms and 60 ms, used in the simulation. These transients were then used to drive the GlyR model of Burzomato et al (2004) (see Supplemental Materials for details), and the resulting traces are shown below. The weighted decay times of these were 8.3 and 16.6 ms. (b) The transient with the 60-ms slow decay constant was used to create the response to 10 stimuli at 100 Hz, resulting in a large buildup of transmitter. The resulting IPSC decayed with a 49.9 ms decay

constant. The gray trace is the scaled response to the single stimulus shown in (a). (c) The glycine transient in (a) was scaled by 0.5 or 2 to simulate an increase or decrease in multivesicular release. Such changes alter peak synaptic responses (indicating that receptors are not saturated by one vesicle) but also change synaptic current decay time. (d) Simulation of IPSCs with the 60 ms slow decay constants and the effects of 300 μM SR-95531. The antagonist both inhibited the IPSC and accelerated its decay. See Supplemental Materials for implementation of antagonist model and further simulations.

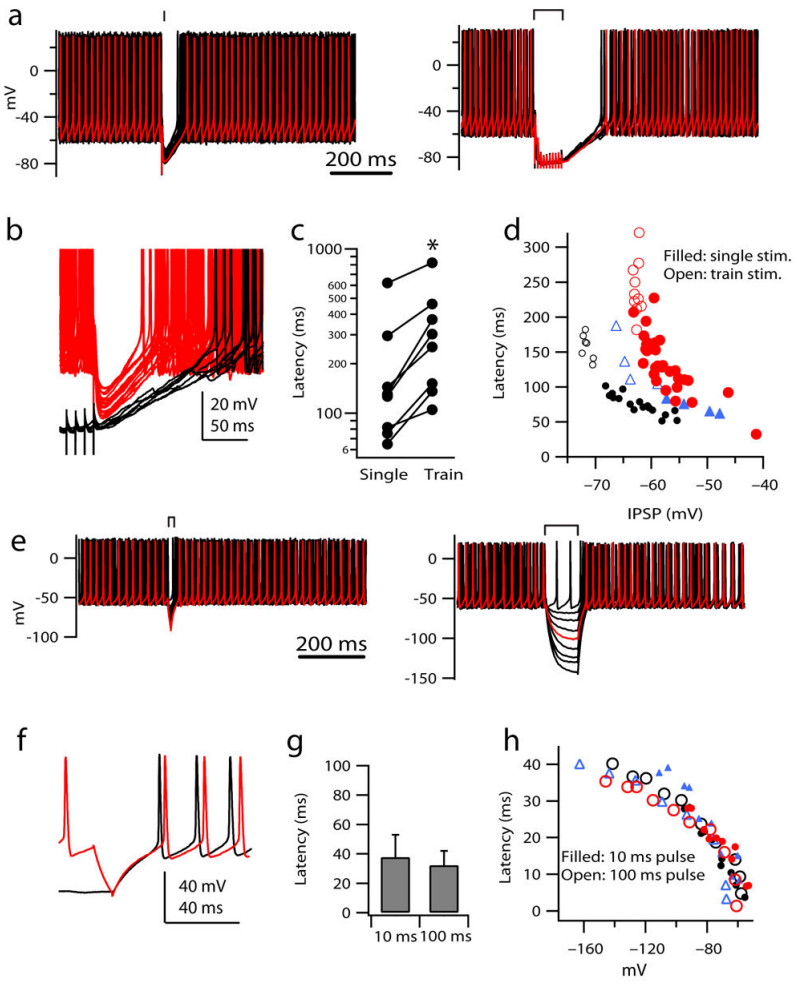

Figure 7. Contribution of IPSC decay time to the duration of inhibition

(a) Example traces showing the duration of inhibition by a single and a train (10 shocks, 100 Hz) of synaptically evoked IPSPs on the granule cell spiking. Black lines at top mark period of the stimuli. Red highlights a single sweep. (b) Traces from panel *a* are overlaid at time of last stimulus. (c) Period between time of last synaptic stimulus and resumption of action potential firing, for single and trains of IPSPs. The latency before spiking resumed increased significantly following a train of IPSPs (n=8; $P < 0.0015$). (d) Relation between peak of negative peak of IPSP and latency to spike firing for three cells. Latency increases sharply with larger IPSPs, consistent with longer lasting synaptic conductance. (e) Example traces in which firing was interrupted by negative current steps (marked by brackets) of different amplitude (range −5 to −50 pA) for 10 ms (left sweeps) or 100 ms (right sweeps). (f) Example of overlaid responses at termination of 10 and 100 ms current pulses that hyperpolarized the neuron to a potential near −80 mV. (g) Latency to spike firing after 10- and 100-ms pulses for IPSPs reaching near −80 mV (−75 mV to −82 mV). (h) Relation between most negative point of hyperpolarization and the resulting latency to firing for six cells. These data show a sublinear relation between voltage and latency suggesting a maximal repriming of A-type K^+ current. Error bars are ±SEM.

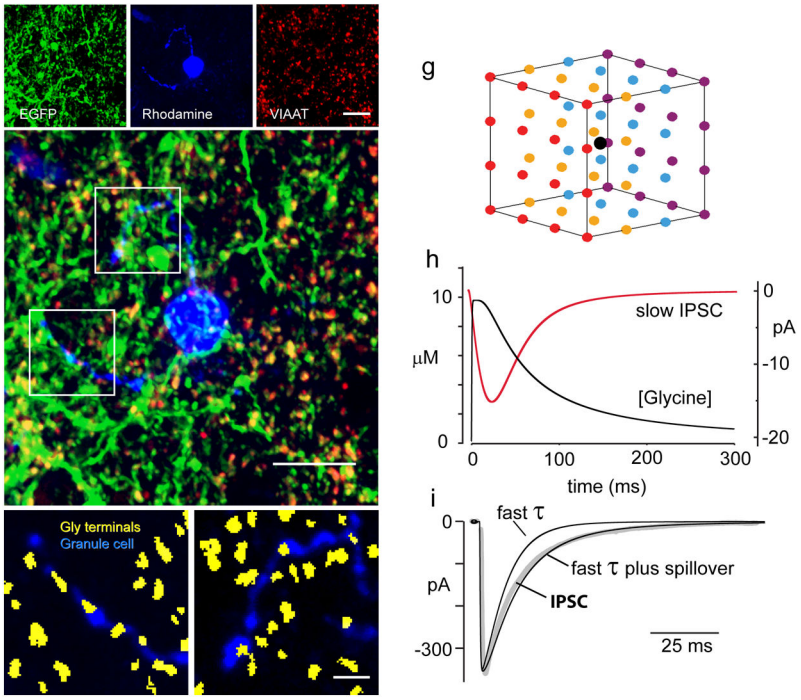

Figure 8. Glycinergic nerve terminal density is consistent with spillover-mediated transmission

(a), EGFP fluorescence in a region of DCN in tissue from a transgenic mouse expressing EGFP in glycinergic neurons. (b), a rhodamine-filled granule cell in the same region as (a). (c), anti-VIAAT antibody signal in the same location as (a) and (b). (d), merged image of (a-c). Regions of overlapping EGFP and VIAAT expression (yellow) were assumed to be glycinergic nerve terminals. (e,f), sample images used for analysis of glycine nerve terminal density from the lower and upper boxed regions in (d), respectively. Yellow regions show colocalized EGFP and VIAAT expression determined by overlaying thresholded EGFP and VIAAT signals (see Methods). The rhodamine-filled granule cell is shown in blue. All images are collapsed stacks of ten adjacent confocal sections acquired 0.2 µm apart in the z-axis. Scale bar in (c) (10 µm) applies to (a-c). Scale bar in (d), 10 µm. Scale bar in (f) (2 µm) applies to (e,f). (g) uniform terminal array in 10 µm cube. Terminals printed in different colors for clarity. (h), Spillover glycine transient (black) summed over all terminals and measured at cube center (black spot in (g)). Red trace is current response to this transient predicted by receptor model. (i), Response of kinetic model (black traces) to fast glycine transient (6 mM peak, 80 usec fast decay, 5 ms-15 µM slow component), to the sum of the fast transient plus the slow transient in panel (h), and a sample IPSC trace (grey). Weighted time constants of these 3 traces were 8.7 ms, 15 ms, and 15 ms, respectively.